Vol 2 No 2 (2020) *e*-ISSN: 2682-8383

Journal of Engineering Technology and Applied Physics

An FPGA based Real-Time Multi-Target Synthetic Aperture Radar Echoes Synthesizer

Chua Ming Yam*, Koo Voon Chet, Lim Heng Siong and Chan Yee Kit
Faculty of Engineering and Technology, Multimedia University, Malaysia.
*mychua@mmu.edu.my
https://doi.org/10.33093/jetap.2020.2.2.2

***Abstract* - This paper proposes a technique for synthesizing multiple point target scatterer Synthetic Aperture Radar (SAR) echoes in real-time. Traditional approaches require high computation resources to calculate the complex SAR echoes due to its complex mathematical model. The proposed technique employs the low computation Direct Digital Synthesis (DDS) approach to generate these complex sinusoid echoes. The proposed Synthetic Aperture Radar Echoes Synthesizer (SAR-ES) is capable of synthesizing SAR echoes accurately in real-time and was built in a Field Programmable Gate Array (FPGA) platform. The system can be used as a testbed to validate and evaluate the performance of a real-time SAR processing algorithms/system prior to the actual flight mission. This could help in reducing the frequency of flight trials and to reduce the SAR system development risk especially for satellite-borne SAR system.**

Keywords— Synthetic Aperture Radar (SAR) echoes, Direct Digital Synthesis (DDS), Field programmable gate array (FPGA)

I. INTRODUCTION

Radar is a common tool used in many applications such as imaging for earth monitoring application, missile guidance in military application, and remote sensing for environmental and weather forecast applications [1, 2]. Synthetic Aperture Radar (SAR) is an active sensor that has its own source of illumination and can operate during day or nighttime, illuminate with variable look angle and cover wide area [3]. The source of a SAR system is a unique signal generated by the transmitter; radiated through the air in the form of electromagnetic wave pulses by the transmitting antenna; reflected by a target and received by the receiving antenna; and finally received by the receiver. The received signal is digitized by the data recorder and stored for further processing. Fig. 1 shows the block diagram of a typical SAR system.

Conventional radar systems digitize the echoes, record and store them in a digital storage media [4]. The data is then retrieved and processed "off-line" for SAR image formation using dedicated signal processing algorithms such as Range Doppler algorithm, Omega-K algorithm, and Chirp Scaling algorithm [5]. However, a modern radar system, with the present of massive on-board processing hardware resources, can process the collected data in real-time during the flight mission. Most seen computing platform used is either digital signal processors (DSP) or field programmable gate array (FPGA) [6, 7], or both [8]. DSP exhibits the advantages in simplicity of usage while FPGA has clear superiority ability in parallel processing.

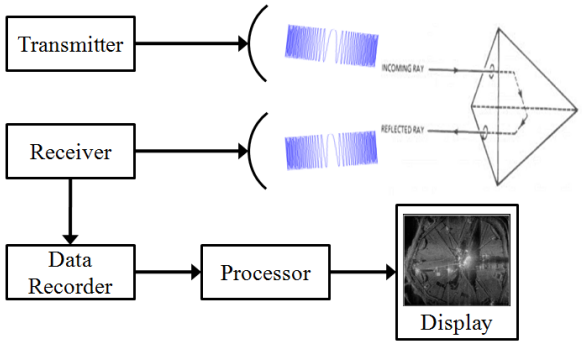

Fig. 1. Block diagram of a Synthetic Aperture Radar system.

Usually, several flight missions are needed to evaluate the effectiveness of a real-time SAR processor. The high running costs and potential risks of a flight mission, with aircraft carrying expensive radar sensor, add difficulties to verify a

Published by MMU PRESS. URL: https://journals.mmupress.com/index.php/jetap/index

real-time SAR signal processor, especially for space-borne SAR system. Therefore, in order to evaluate the performance of a SAR signal processor or images formation chain, generation of echoed SAR signals is essential. The traditional approach of SAR signal simulation using computer is useful for SAR system design, analysis, and algorithm development. However, computer-based simulation is not capable of evaluating the performance of an actual SAR signal processor that runs in real-time.

Radar echo simulator plays an important role in the design and development of a real-time SAR signal processor. This is a hardware simulator platform having the ability to provide real-time SAR echoed signal for verifying and analyzing the effectiveness of real-time SAR signal processor and real-time SAR signal processing algorithm. It can greatly minimize the cost of flying test for air-borne SAR [9] system, ISAR [10] or space-borne radar system. Some examples of radar simulator can be found in technical literature papers as described in [8, 11 – 14].

A practical SAR signal generator should be able to synthesize radar raw signals in real-time and can be seamlessly integrated with the onboard radar subsystems to form a complete SAR signal-processing unit. It can be used to evaluate and test the functionality of the entire SAR system prior to the actual launching, as well as during the flight mission as part of the system verification processes. In this paper, a method of synthesizing SAR echoed signal using Direct Digital Synthesis (DDS) technique is proposed. As compared to the conventional waveform generation techniques (analog, Phase-Locked Loop, arbitrary waveform generation), DDS technique offers several advantages such as, superior frequency tuning digitally, high waveform reconfiguration flexibility, fast tuning response time, and low computation power requirements [15]. Due to the simplicity of DDS approach in generating complex sinusoid signal (DDS requires only an accumulator and phase-to-amplitude mapping), the proposed method does not require high computation power. The proposed system is an extension to the existing SAR system developed by Multimedia University Malaysia [16] and does not require hardware level modification for implementation. In-lab testing shows that the signal generator is capable of synthesizing point target SAR echoed signal accurately, in real-time.

II. Synthetic Aperture Radar Signals

A SAR system uses Linear Frequency Modulated (LFM) pulse, or commonly known as "*Chirp*" pulse [17], as the unique signal identity during signal recognition. The baseband chirp signal can be expressed as,

$$x_b(t) = A \cdot \Pi\left(\frac{t}{T}\right) \cdot e^{j\pi\left(\alpha t^2 - Bt\right)} \tag{1}$$

where,

A = peak-to-peak amplitude of the chirp signal
α = the chirp rate
B = the chirp bandwidth

$$\Pi\left(\frac{t}{T}\right) = \begin{cases} 1 & for\ 0 \le t \le T \\ 0 & elsewhere \end{cases}$$

T = the chirp pulse width

An example of a chirp signal with bandwidth of 80 MHz and pulse width of 10μs plotted in time- and frequency-domain is shown in Fig. 2(a) and Fig. 2(b), respectively.

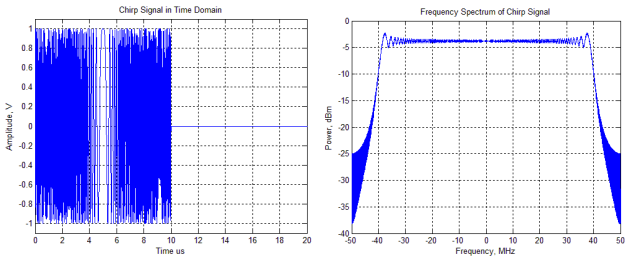

(a) (b)

Fig. 2. Baseband chirp signal in (a) Time domain. (b) Frequency domain.

Usually, the baseband chirp signal is up-converted to carrier band prior to actual transmission. The up-converted baseband chirp signal to the carrier frequency, f_c, can be expressed as,

$$x(t) = A \cdot \Pi\left(\frac{t}{T}\right) \cdot e^{j\pi\left(\alpha t^2 - Bt\right)} \cdot e^{j2\pi f_c t} \tag{2}$$

III. The Synthetic Aperture Radar Echoes

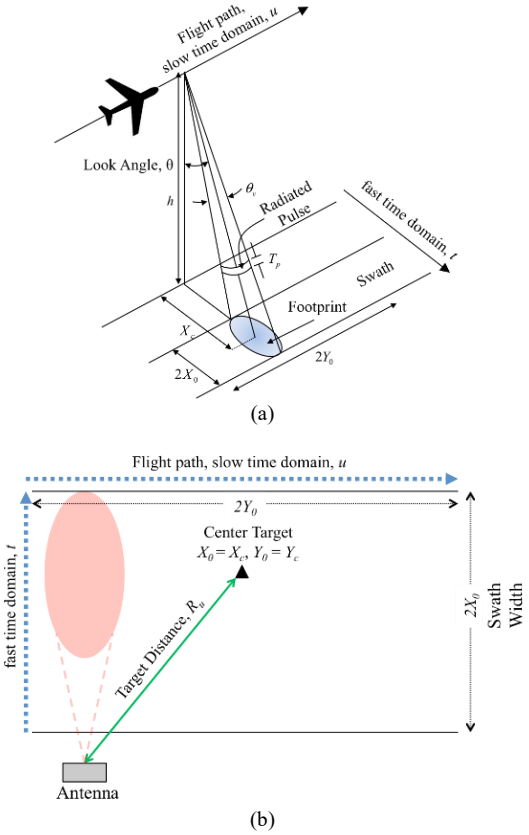

(a)

(b)

Fig. 3. Basic principles of Synthetic Aperture Radar.

SAR uses the forward motion of its platform to synthesize an extremely large synthetic antenna. Fig. 3 depicts the basic

operating principles of a SAR system. While the sensor is moving in the slow time domain, *u*, at each Pulse Repetition Interval (PRI) interval, a pulse will be transmitted in the fast time domain, *t*. A portion of the transmitted pulses will be reflected by the target (also known as delayed replica of the transmitted chirp), collected by the receiver, and finally recorded by the SAR sensor. The sensor will then accumulate an array of the delayed transmitted chirp replica and store them in digital storage for further processing. Using special signal processing algorithm, high-resolution remote sensing imagery could be generated.

The delayed chirp replica from a single point target can be modeled from the baseband chirp equation (Eq. (2)). Since the replica is a delayed version of its transmitted chirp pulse, hence, the fast time in the chirp replica, t_d, is then,

$$t_d = t - \tau \tag{3}$$

where $\tau = \frac{2R}{c}$ is the round-trip time delay of the target, R is the range of the target, and c is speed of light.

Substituting Eq. (3) into Eq. (2), the chirp echoed signal reflected by a single target could be formulated as,

$$\begin{aligned} x_{echoed}(t_d) &= A_r \cdot \Pi\left(\frac{t-\tau}{T}\right) \cdot e^{j\pi\left(\alpha(t-\tau)^2\right) - B(t-\tau)} \cdot e^{j2\pi f_c(t-\tau)} \\ &= A_r \cdot \Pi\left(\frac{t-\tau}{T}\right) \cdot e^{j\pi\left(\alpha t^2 - Bt + 2f_c t - 2\alpha t\tau + \alpha\tau^2 + B\tau - 2f_c\tau\right)} \end{aligned} \tag{4}$$

Down-converting the echoed chirp pulse to baseband, and mixing it with the carrier, gives,

$$x_{echoed_b}(t_d) = A_r \cdot \Pi\left(\frac{t-\tau}{T}\right) \cdot e^{j\pi\left(\alpha t^2 - Bt - 2\alpha t\tau + \alpha\tau^2 + B\tau - 2f_c\tau\right)} \tag{5}$$

Hence, the instantaneous phase, $\varphi(t)$, of the baseband echoed chirp pulse can be de-composed into,

$$\phi_{echoed\_b}(t_d) = \pi\left(\underbrace{\alpha t^2 - Bt}_{\text{baseband transmitted signal}} \quad \underbrace{-2\alpha t\tau}_{\text{frequency shift component}} \quad \underbrace{+\alpha\tau^2 + B\tau - 2f_c\tau}_{\text{phase shift component}} \right) \tag{6}$$

The equation above shows that the instantaneous phase of the baseband echoed chirp signal reflected by a single target is a composition of 3 components: i) the baseband transmitted signal, ii) a frequency shift component, and, iii) a phase shift component. As compared to the instantaneous phase of the transmitted signal, two additional components were induced in the instantaneous phase of the baseband echoed signal, as the result of round-trip electromagnetic wave propagation of the transmitting SAR signal.

If there are *n* numbers of target within the illumination area of the sensor, the echoed signal will then become the summation of each individual echoed pulses. Mathematically, it can be represented as,

$$x_{echoed\_b}(t_d) = \sum_{k=0}^{n} A_k \cdot \Pi\left(\frac{t-\tau_k}{T}\right) \cdot e^{j\pi\left(\alpha t^2 - Bt - 2\alpha t\tau_k + \alpha\tau_k^2 + B\tau_k - 2f_c\tau_k\right)} \tag{7}$$

Considering the slow-time domain, *u*, into Eq. (7), which models the changes of the target's range as the platform moves,

$$x_{echoed\_b}(u,t_d) = \sum_{k=0}^{n} A_{u,k} \cdot \Pi\left(\frac{t-\tau_{u,k}}{T}\right) \cdot e^{j\pi\left(\alpha t^2 - Bt - 2\alpha t\tau_{u,k} + \alpha\tau_{u,k}^2 + B\tau_{u,k} - 2f_c\tau_{u,k}\right)} \tag{8}$$

As a summary, the baseband echoed SAR signal is synthesizable by adding three additional components into the transmitting SAR signal, which are: i) a frequency shift component, ii) a phase shift component, and iii) a time shift component. These additional components can be related to the distance from the antenna to the target, *R*, as shown in Eq. (8).

IV. SAR Echoes Generation using Direct Digital Synthesis (DDS) Technique

Direct Digital Synthesis is a method of producing an analog waveform, usually a sinusoid, by generating a time-varying signal in digital form and then performing a digital-to-analog conversion. Recently, DDS has been widely used in radar waveform synthesis due to its flexibility in radar waveform re-configuration without the needs of hardware re-configuration. Detailed operating principle of a DDS waveform generator for SAR system can be found in [6, 17].

Basically, DDS is based upon the phase-frequency relationship in a sinusoidal signal [18]. A complete sine-wave oscillation can be visualized as a rotating vector that rotates around a phase circle from 0° to 360°. When the rotating vector is rotating at constant speed, sine-wave linear phase information is produced. Since the output frequency is a function of the number of steps to complete a wheel cycle, the number of discrete phase points contained in the wheel (the length of the phase accumulator) is determined by the resolution, a modulus 2^n, of the phase accumulator.

The phase accumulator increments its stored number each time it receives a clock pulse. The magnitude of the increment is determined by a digital tuning word, *M*. The tuning word forms the phase step size between reference clock updates. The relationship of the phase accumulator and tuning word forms the DDS equation, which gives the output frequency [17],

$$f_{out} = \frac{M \times f_c}{2^n} \tag{9}$$

where f_c is the internal clock frequency for the DDS core, 2^n is the size of the accumulator.

A chirp could be generated using a DDS core. First, the windowing function can be implemented by time gating the digital output of the DDS core with a pulse-gating signal. Then the instantaneous frequency of the radar waveforms can be altered by changing the DDS core tuning word, *M*, at every

elapsed clock tick. For chirp signal generation, the instantaneous tuning word, M_i, can be derived from baseband chirp equation (Eq. (1)) as,

$$M_i = \frac{\left(\alpha t - \frac{B}{2}\right) \times 2^n}{f_c} \tag{10}$$

It is shown in Eqs. (5) and (6) that the echoed chirp signal is composed of an original transmitted signal, a frequency shift component, a phase shift component, and a time shift component. For SAR echoes synthesis, the DDS core is modified to receive the additional inputs, rather than just the tuning word, M_i. A modified DDS core for a single target is shown in Fig. 4 where the core accepts all configuration data. The configuration data are the baseband chirp tuning word, M_{b_i}, the frequency shift word, M_{f_i}, the phase shift word, M_{p_i}, and the time shift word, M_{t_i}. The above-mentioned data can be generated from the following equations,

$$M_{b\_i} = \frac{(\alpha\tau - \frac{B}{2}) \times 2^n}{f_c}, \; M_{f\_i} = \frac{(-\alpha\tau) \times 2^n}{f_c}$$
$$M_{p\_i} = \alpha\tau^2 + B\tau - 2f_c\tau \bmod 2^{n_a}, \; M_{t\_i} = t - \tau f_c \tag{11}$$

Using the proposed DDS core, by calculating the configuration data at every clock tick, the echoed signal for a single target is synthesizable, in real-time. For the formation of multiple targets SAR echoed signal, the echoed signal for each of the target will be summed prior to the conversion to analog representation. A dedicated single target DDS core will synthesize the echoed signal for each of the target.

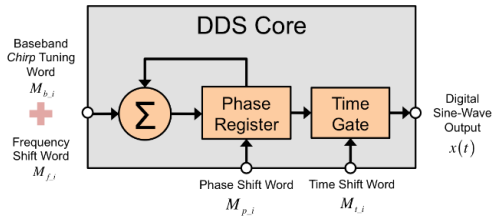

Fig. 4. Modified single target DDS core for SAR-ES.

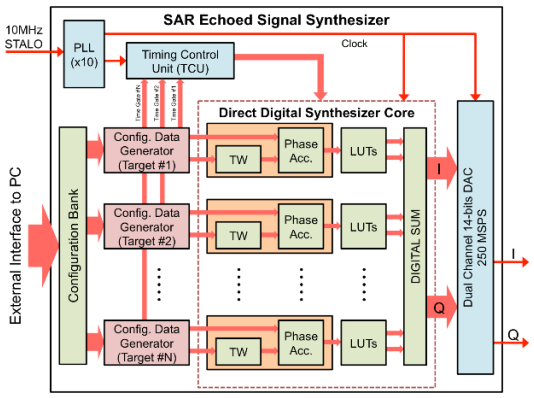

Fig. 5. Block diagram of SAR-ES.

Fig. 6 depicts the proposed SAR-ES hardware layer architecture. The SAR-ES consists of multiple Single Target SAR-ES DDS core, each which has its own configuration data generator. The data generator generates the entire configuration data needed by the DDS core as described in Eqs. (9) to (11). Each of the target information could be re-configured through the external UART (Universal Asynchronous Receiver/Transmitter) interface to a computer system. The digital data generated by the single target DDS core will be combined using a digital sum to form the final echoed signal. It is then converted to analog representation using a Digital-to-Analog Converter (DAC). The Timing and Control Unit (TCU) will generate all internal timing signals.

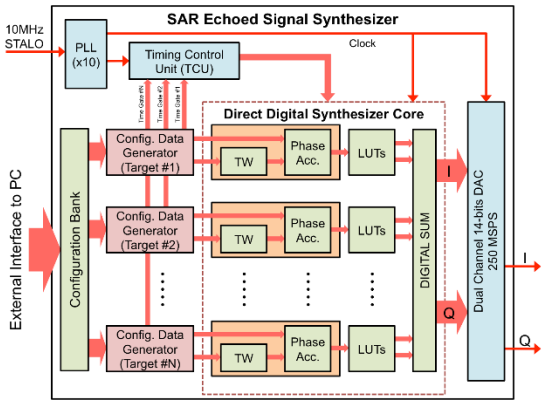

Fig. 6. Block diagram of SAR-ES.

V. Simulation of SAR Echoes

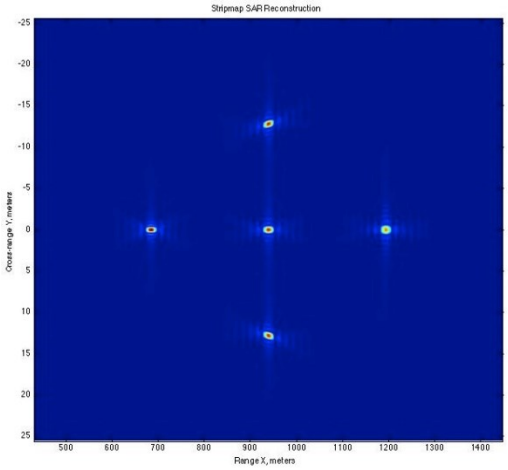

(a)

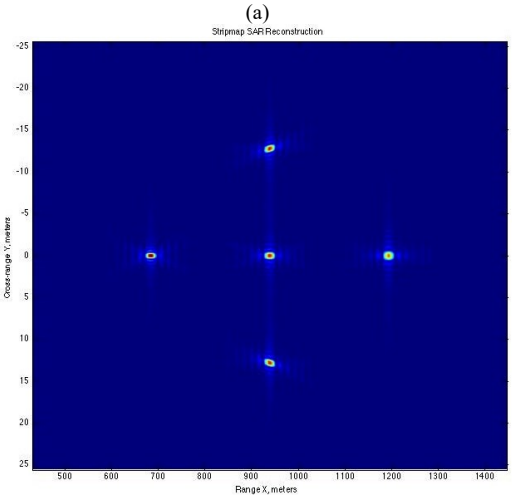

(b)

Fig. 7. Reconstructed SAR images: (a) Equation generated SAR echoed signal and (b) DDS generated SAR echoed signal.

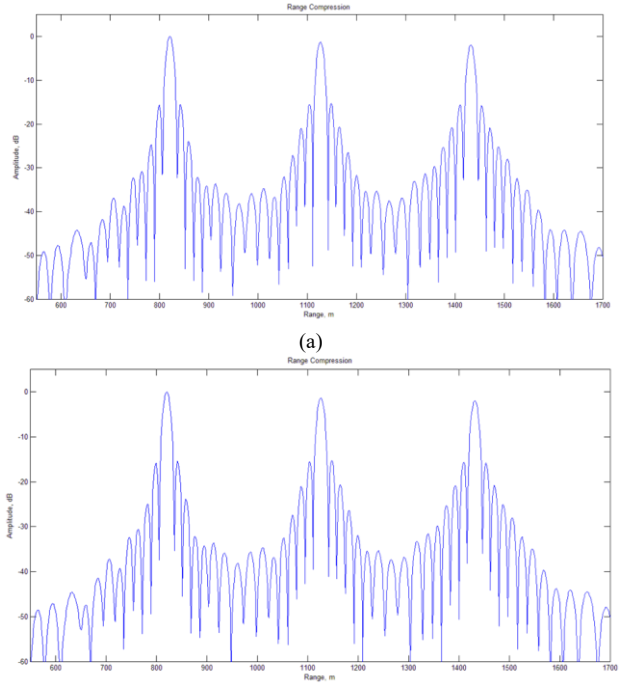

(a)

(b)

Fig. 8. Range compressed signal at cross range center: (a) Equation generated SAR echoed signal and (b) DDS generated SAR echoed signal.

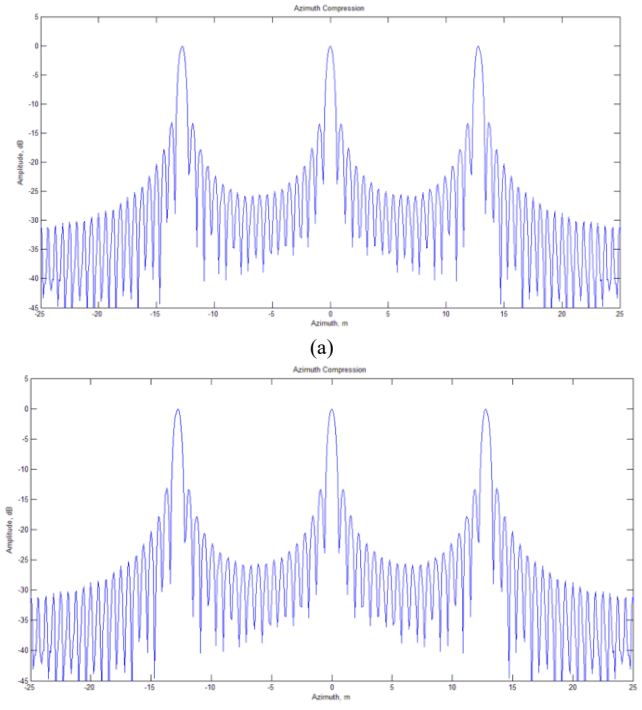

(a)

(b)

Fig. 9. Cross-range compressed signal at range center: (a) Equation generated SAR echoed signal and (b) DDS generated SAR echoed signal.

In order to verify the functionality of the proposed method, the method was simulated in Matlab® prior to the implementation into FPGA platform. Two echoed signals were generated for comparison purpose, one using the proposed method while another using the modeled equation (ideal echoed signal). A similarity comparison on both the echoed signals was carried out. Figure 7 shows the re-constructed image for both the signals. Fig. 88 shows the range-compressed signal at the center of cross-range bin and Fig. 9 shows the cross-range compressed signal at the center of a range bin. The results show that the echoed signal generated using the proposed method is identical to the echoed signal generated using the mathematical model.

VI. Hardware Implementation on FPGA Platform

The proposed SAR-ES architecture was implemented in Intel (previously known as Altera) DSP Development board (Stratix III Edition). To convert the digital data into analog, an Intel Data Conversion Card was used. Meanwhile, for data recording, the same embedded real-time data collector was employed [4]. Table I summarizes the specifications of hardware used.

Table I. Hardware specifications.

Module	Specifications
Altera DSP Development Board (Stratix III Edition)	Altera EP3SL150F1152 FPGA 142500 LEs 6,390 kbits memory 384 18x18-bit multipliers 8 PLLs 744 I/O
Terasic AD/DA Data Conversion Card	Channel: 2 Resolution: 14-bit Sampling rate: 250 MSPS

The collected data is then processed for image re-construction and finally, the image obtained is compared with the ideal image obtained from Matlab® simulation. Fig. 1010 shows the entire measurement setup for data collection.

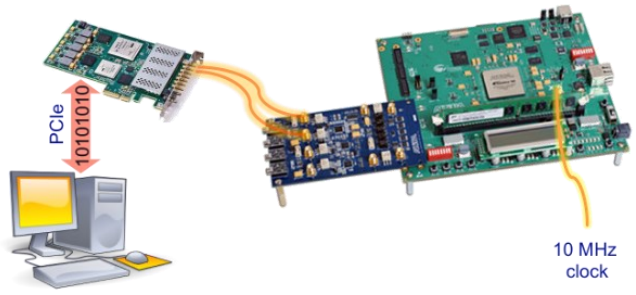

Fig. 10. Measurement setup.

Fig. 11, 12 and 13 shows the comparison between the echoed signal generated using Matlab® and FPGA platform. Both the images in Fig.11 appeared to be the same. However, from the range and the cross-range (Figs. 11 & 12) compressed signal, some noise is observed near the noise floor of the signal. The noise observed is mainly contributed by the DAC during digital-to-analog conversion.

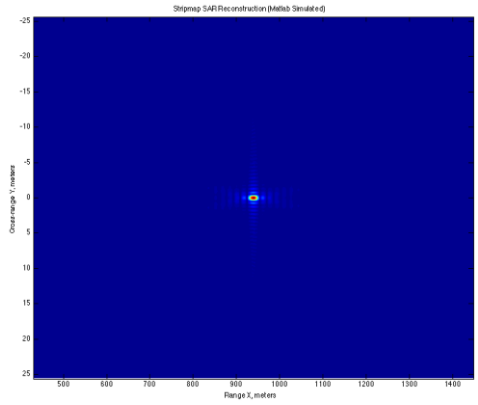

(a)

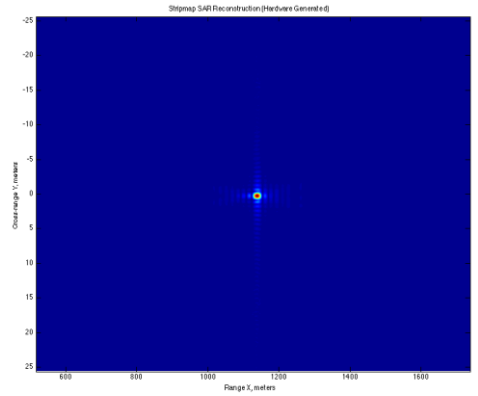

(b)

Fig. 11. Re-constructed image: (a) Matlab® simulated and (b) Hardware generated.

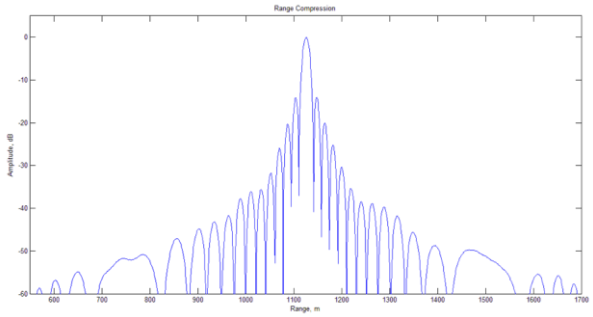

(a)

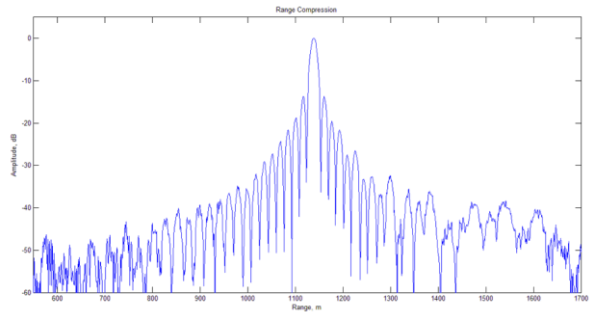

(b)

Fig. 12. Range compressed signal at cross range center: (a) Matlab® simulated and (b) Hardware generated.

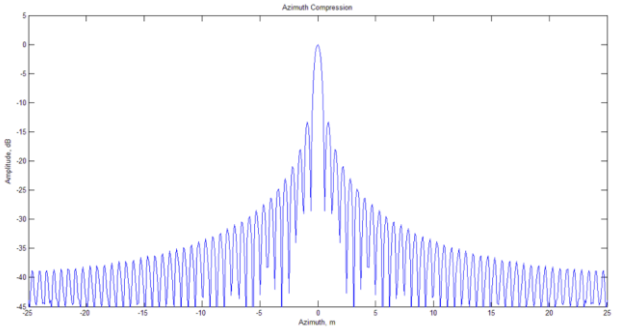

(a)

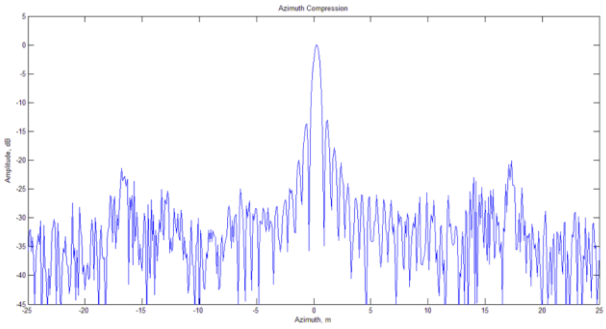

(b)

Fig. 13. Cross-range compressed signal at range center: (a) Matlab® simulated and (b) Hardware generated.

Table II summarizes the SAR image quality assessment for all the echoed signals generated from the point of view of the Peak Side Lobe Ratio (PSLR) and the Integrated Side Lobe Ratio (ISLR) of the compressed waveform. The data shows that the re-constructed image quality of the hardware generated echoed signal has is comparable to the simulated echoed signals.

VII. CONCLUSION

In this paper, a new technique of synthesizing SAR echoes has been proposed. The proposed technique does not require massive Digital Signal Processing (DSP) computing power as compared to currently available solution. Comparison study on the proposed technique with the mathematical model shows that the proposed technique can accurately synthesize the SAR echoes. The technique is implemented in an FPGA system to generate SAR echoes in real time and can be used as a testbed for SAR processor validation prior to the actual flight mission.

ACKNOWLEDGEMENT

This project is funded by TM R&D research grant.

Table. II. Summary of SAR image quality assessment for the generated echoed signal.

Parameters		Matlab® Simulated (Mathematics) Equation)	Matlab® Simulated (Proposed method)	Hardware Generated (Proposed method)
Peak Side Lobe Ratio (PSLR)	Range	-14.6225 dB	-14.5238 dB	-13.7092 dB
	Cross-Range	-13.4793 dB	-13.4784 dB	-13.0485 dB
Integrated Side Lobe Ratio (ISLR)	Range	-58.6040 dB	-56.7590 dB	-59.0234 dB
	Cross-Range	-58.6884 dB	-57.4095 dB	-58.9815 dB

REFERENCES

[1] M. I. Skolnik, *Radar Handbook*, New York: McGraw-Hill, 1970.

[2] M. Y. Chua, J. T. Sri Sumantyo, C. E. Santosa, G. F. Panggabean, D. Sri Sumantyo, T. Watanabe, Y. Q. Ji, P. P. Sitompul, M. Nasuc F. Kurniawan, B. Purbantoro, A. Awaludin, K. Sasmita, E. Rahardji, G. Wibisono, R. H. Jatmiko, Sudaryatno, T. H. Purwanto, S. Widartono and M. Kamal, "The Maiden Flight of Hinotori-C: T First C Band Full Polarimetric Circularly Polarized Synthetic Apertu Radar in The World," *IEEE Aerospace and Electronic Syste Magazine,* vol. 34, no. 2, pp. 24-35, 2019.

[3] Y. K. Chan and V. C. Koo, "An Introduction to Synthetic Apertu Radar," *Progress in Electromagnetic Research B,* vol. 2, pp. 27-(2008.

[4] C. H. Lim, C. S. Lim, M. Y. Chua, Y. K. Chan, T. S. Lim and V. Koo, "A New Data Acquisition and Processing System UAVSAR," *IEICE Electronics Express,* vol. 8, no. 20, pp. 1716-17 2011.

[5] A. Moreira, P. Prats-Iraola, M. Younis, G. Krieger, I. Hjansek and P. Papathanassiou, "A Tutorial on Synthetic Aperture Radar," *IE Geoscience and Remote Sensing Magazine,* vol. 1, no. 1, pp. 6-4 2013.

[6] M. Y. Chua, H. S. Boey, C. H. Lim, V. C. Koo, H. S. Lim, Y. K. Ch and T. S. Lim, "A Miniature Real-time Re-configurable Rac Waveform Synthesizer for UAV Based Radar," *Progress Electromagnetics Research C,* vol. 31, pp. 169-183, 2012.

[7] M. Y. Chua, V. C. Koo, H. S. Lim and J. T. Sri Sumantyo, "Phas coded Stepped Frequency Linear Frequency Modulated Wavefo Synthesis Technique for Low Altitude Ultra-wideband Synthe Aperture Radar," *IEEE Access,* vol. 5, pp. 11391-11403, 2017.

[8] B. P. Hawkins and W. Tung, "UAVSAR Real-Time Embedded GI Processor," in *2019 IEEE International Geoscience and Remo Sensing Symposium*, Yokohama, 2019.

[9] A. Kozme and J. Walker, "Synthetic Aperture Radar Technology Application," in *Engineering Summer Conferences*, Michigan.

[10] M. Soumekh, "A System Model and Inversion for Synthetic Aperture Radar Imaging," *IEEE Transactions on Image Processing,* vol. 1, no. 1, pp. 64-76, 1992.

[11] K. Radecki, P. Samczyński, K. Kulpa and J. Drozdowicz, "A real-Time Unfocused SAR Processor Based on A Portable CUDA GPU," in *2015 European Radar Conference (EuRAD)*, Paris, 2015.

[12] B. Li, C. Li, Y. Xie, L. Chen, H. Shi and Y. Deng, "2018 IEEE High Performance Extreme Computing Conference (HPEC)," in *A SoPC based Fixed Point System for Spaceborne SAR Real-Time Imaging Processing*, Waltham, 2018.

[13] Y. Sugimoto, S. Ozawa and N. Inaba, "Near Real-Time Sar Image Focusing Onboard Spacecraft," in *2018 IEEE International Geoscience and Remote Sensing Symposium*, Valencia, 2018.

[14] N. Zhang, D. Yao, C. Li and K. Jing, "A Real-Time Processing System for Airborne Forward-Squint SAR Based on DSP," in *IET International Radar Conference 2015*, Hangzhou, 2015.

[15] B. Cronin, "DDS Devices Generate High-Quality Waveforms Simply, Efficiently, and Flexibly," *Analog Dialogue,* 2012.

[16] V. C. Koo, Y. K. Chan, V. Gobi, M. Y. Chua, C. H. Lim, C. S. Lim , C. C. Thum, T. S. Lim, Z. Ahmad, K. A. Mahmood, M. H. Shahid, C. Y. Ang, W. Q. Tan, P. N. Tan, K. S. Yee, W. G. Cheaw, H. S. Boey, A. L. Choo and B. C. Sew, "A New Unmanned Aerial Vehicle Synthetic Aperture Radar for Environmental Monitoring," *Progress in Electromagnetics Research,* vol. 122, pp. 245-268, 2012.

[17] M. Y. Chua and V. C. Koo, "FPGA-based Chirp Generator for High Resolution UAV SAR," *Progress In Electromagnetics Research,* vol. 99, pp. 71-88, 2009.

[18] Analog Devices, "A Technical Tutorial on Digital Signal Synthesis," Analog Devices, 1999.